

Unified direct parameter estimation via quantum reservoirs

Yinfei Li,¹ Sanjib Ghosh,^{2,*} Jiangwei Shang,^{1,†} Qihua Xiong,^{2,3} and Xiangdong Zhang¹

¹*Key Laboratory of Advanced Optoelectronic Quantum Architecture and Measurement of Ministry of Education, School of Physics, Beijing Institute of Technology, Beijing 100081, China*

²*Beijing Academy of Quantum Information Sciences, Beijing 100193, China*

³*State Key Laboratory of Low-Dimensional Quantum Physics and Department of Physics, Tsinghua University, Beijing 100084, China*

(Dated: June 1, 2023)

Parameter estimation is an indispensable task in various applications of quantum information processing. To predict parameters in the post-processing stage, it is inherent to first perceive the quantum state with a measurement protocol and store the information acquired. In this work, we propose a general framework for constructing classical approximations of arbitrary quantum states with quantum reservoir networks. A key advantage of our method is that only a single local measurement setting is required for estimating arbitrary parameters, while most of the previous methods need exponentially increasing number of measurement settings. To estimate M parameters simultaneously, the size of the classical approximation scales as $\ln M$. Moreover, this estimation scheme is extendable to higher-dimensional systems and hybrid systems with non-identical local dimensions, which makes it exceptionally generic. Both linear and nonlinear functions can be estimated efficiently by our scheme, and we support our theoretical findings with extensive numerical simulations.

I. INTRODUCTION

Parameter estimation plays a central role in the implementation of various quantum technologies, such as quantum computing, quantum communication and quantum sensing. This highlights that extracting information from a quantum system to a classical machine lies at the heart of quantum physics. The prominent technique for this task, quantum tomography, studies the reconstruction methods of density matrices for quantum states. The density matrix captures all the information of a quantum system, and is useful in predicting properties of it. However, the curse of dimensionality has emerged with the advent of the noisy intermediate-scale quantum (NISQ) era [1], which renders it infeasible to obtain a complete description of quantum systems with a large number of constituents. Moreover, a full description is often superfluous in tasks where only key properties are relevant. As a consequence, the concept of shadow tomography is proposed to focus on predicting certain properties of a quantum system [2].

A particularly important progress in the study of shadow tomography is the advancement of randomized measurements [3, 4], the virtue of which is highlighted as “*Measure first, ask questions later*” [5]. The randomized measurement protocols proposed by Huang, Kueng and Preskill construct approximate representations of the quantum system, namely classical shadows, via Pauli group and Clifford group measurements [4]. The single-snapshot variance upper bound of classical shadows is determined by the so-

called shadow norm, which is asymptotically optimal for global measurements. In addition, the statistical fluctuation can be further suppressed by constructing classical shadows with positive operator-valued measures (POVMs) [6–8]. The classical shadows are highly efficient in the estimation of various properties in the post-processing phase, the benefits of which extend to entanglement detection [9], characterization of topological order [10], machine learning for many-body problems [11], etc. However, these protocols pose a challenge in experiments due to the need for exponentially increasing measurement settings to achieve an arbitrary accuracy. Hence, various techniques are introduced to tackle this problem [12–15]. Moreover, the theoretical results are based on the fact that multi-qubit Clifford groups are unitary 3-designs [16], which is not the case for arbitrary qudit systems. The generalization of these results to higher-dimensional systems typically require complex unitary ensembles that are hard to implement [17–20]. Therefore, a general method for direct estimation with a single measurement setting is highly desirable.

Recently, quantum neural networks [21–23] are widely studied as promising artificial neural networks due to their enhanced information feature space supported by the exponentially large Hilbert space [24, 25]. Unlike traditional computing frameworks, neural networks learn to perform complex tasks based on training rather than predefined algorithms or strategies [26]. With the capacity to produce data that displays atypical statistical patterns, quantum neural networks have the potential to outperform their classical counterparts [22]. However, training a quantum neural network can be equally hard [27]. Indeed, it has been shown that training of quantum neural networks could be exceptionally difficult owing to the

* sanjibghosh@baqis.ac.cn

† jiangwei.shang@bit.edu.cn

barren plateaus or far local minima in the training landscapes [28–31]. This is the reason that quantum neural networks are often limited to shallow circuit depths or small number of qubits. A trending line of research that circumvents this issue is quantum reservoir processing (QRP) [32–34], which is a quantum analogy of recurrent networks.

In this work we present a direct parameter estimation scheme via quantum neural networks, which overcomes the obstacles faced by randomized measurement protocols by harnessing the richness of QRP. In QRP, training is completely moved out of the main network to a single output layer, such that the training becomes a linear regression eliminating the possibility of producing barren plateaus or local minima. Such a quantum neural network retains its quantum enhanced feature space while being trainable via a fast and easy mechanism. Based on this efficiently trainable QRP, we establish a unified measurement protocol for direct quantum parameter estimations. A scheme of minimal quantum hardware comprising pair-wise connected quantum nodes is developed to estimate arbitrary parameters of a quantum state. As major advantages, our scheme requires single-qubit measurements, only in a single setting, and a logarithmic network size $\sim \ln d$ with respect to the dimension d of the input state. All of these are particularly favorable for actual physical implementations.

Furthermore, we establish rigorous performance guarantee by adopting the mindset of shadow estimation. According to Born’s rule, one measurement of a quantum state is analogous to sampling a probability distribution once. Thus, learning properties of a quantum state involves measuring identical and independently distributed (i.i.d.) samples of the quantum state a certain number of times. To estimate M observables of the state within an additive error ϵ and with constant confidence, the number of i.i.d. input samples consumed scales as $O(F_{\text{res}} \ln M / \epsilon^2)$. The factor F_{res} represents the variance upper bound of the single sample estimator, which depends solely on the observables and the reservoir dynamics, and its magnitude is comparable to that of the shadow norm. As a direct consequence of the pair-wise reservoir dynamics, F_{res} for a k -local observable is the product of that for each single-qubit observable. We support the theoretical results with extensive numerical simulations.

II. QUANTUM RESERVOIR PARAMETER ESTIMATION

In this section we introduce the scheme of quantum reservoir parameter estimation (QRPE), which evaluates physical properties of input quantum states based on a quantum estimation device. Our goal parallels that of shadow estimation: to devise a resource-efficient classical representation of complex quantum states that permits access to their properties through subsequent classical processing.

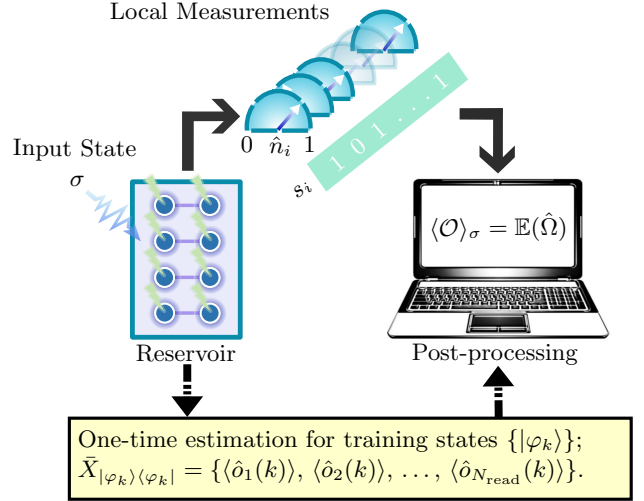


FIG. 1. Schematic illustration of direct parameter estimation with quantum reservoirs. A source prepares an n -qubit quantum state σ which is taken as input by a pair-wise reservoir network with $2n$ qubits. For the i -th input copy, the local measurement operator on the j -th node is $\hat{n}_j = (\mathbb{1} - \zeta_j^z)/2$, and the readout is a bit string $s_i \in \{0, 1\}^n$, corresponding to one of the N_{read} readout operators. Equipped with the training data, an unbiased estimator $\hat{\Omega}$ is constructed for the parameter \mathcal{O} .

A. Physical setting

We consider a system based on interacting quantum nodes which is used as a dynamical estimation device. More specifically, our considered device is a pair-wise connected network of qubits, as shown in Fig. 1, where the connections are obtained with transverse exchange interactions [35] and each qubit is excited with a continuous driving field. For n -qubit input states, there are n pairs of reservoir nodes. The corresponding Hamiltonian of the qubit network device is given by

$$\hat{H} = \sum_{i=1}^n \left[J(\zeta_{2i-1}^x \zeta_{2i}^x + \zeta_{2i-1}^y \zeta_{2i}^y) + P_1 \zeta_{2i-1}^x + E_1 \zeta_{2i-1}^z + P_2 \zeta_{2i}^x + E_2 \zeta_{2i}^z \right]. \quad (1)$$

The operators $\zeta_i^{x,y,z}$ represent the Pauli operators on the i -th quantum node, which has a compatible dimension with the context. The parameter J represents the strength of the pair-wise transverse exchange interaction between $(2i-1)$ -th and $2i$ -th nodes. The parameters $P_{1,2}$ and $E_{1,2}$ represent driving field strength and onsite energy respectively. Such a device can be readily realized with superconducting qubits, where the exchange interaction can be realized via a cavity quantum bus [35]. Moreover, the form of \hat{H} is of a quantum spin Hamiltonian which can be realized in a variety of platforms such as NMR [36, 37], quantum dots [38], and trapped ions [39].

B. Measurement protocol

To estimate properties of a quantum state σ , it is injected into the quantum reservoir via an invertible map, which for simplicity we choose the SWAP operations. Thus, the initial state of the network at time $t = 0$ is given by the density matrix: $\rho(0) = \sigma \otimes [|0\rangle\langle 0|]_{\text{rest}}$, where the suffix ‘rest’ indicates the network nodes other than the ones connected to the input qubits via the SWAP gates. The initial reservoir state evolves in time as,

$$\rho(t) = \hat{U}^\dagger(t)\rho(0)\hat{U}(t), \quad (2)$$

where $\rho(t)$ is the density operator at time t and $\hat{U}(t) = \exp(-it\hat{H}/\hbar)$ is the evolution operator. After a sufficient time evolution, we perform local Pauli-Z measurements on the reservoir nodes (qubits). For each node there are two readouts +1 and -1, represented by the projectors onto the positive and negative eigen subspace of Pauli-Z operator $\{\zeta_i^z\}$ respectively. The final readouts are provided by a set of commuting readout operators

$$\begin{aligned} \{\hat{o}_i\} &= \prod_{j=1}^{N_{\text{node}}} \left\{ \frac{\mathbb{1} - \zeta_j^z}{2}, \frac{\mathbb{1} + \zeta_j^z}{2} \right\} \\ &= \{\hat{C}_\emptyset\} \cup \{\hat{C}_{\{i_1\}}\} \cup \{\hat{C}_{\{i'_1, i'_2\}}\} \cup \dots, \end{aligned} \quad (3)$$

where N_{node} is the number of reservoir nodes. \hat{C}_S is an element of the set $\{\hat{o}_i\}$, which is related to the Pauli-Z operators as

$$\hat{C}_S = \prod_{i \in S} \frac{\mathbb{1} - \zeta_i^z}{2} \prod_{j \notin S} \frac{\mathbb{1} + \zeta_j^z}{2}, \quad (4)$$

so it represents the configuration of measurement outcomes that only nodes in the set S result in -1 for local Pauli-Z measurements. Hence, the readout for the i -th input is recorded by a bit string $s_i \in \{0, 1\}^n$. The total number of readout operators in $\{\hat{o}_i\}$ is given by

$$N_{\text{read}} = \sum_{k=0}^{N_{\text{node}}} \binom{N_{\text{node}}}{k} = 2^{N_{\text{node}}}, \quad (5)$$

where $\binom{N_{\text{node}}}{k}$ is the combinatorial number.

Considering that $\{\hat{o}_i\}$ forms an orthogonal measurement basis with a total number of $2^{N_{\text{node}}}$ elements, a reservoir with a minimal of $N_{\text{node}} = 2 \log_2 d$ nodes is required to estimate arbitrary quantum parameters for input states supported on a d -dimensional Hilbert space \mathcal{H}_d . This observation agrees with our proposal of pair-wise connected reservoir networks. Moreover, the commutativity of the chosen readout operators leads to quantum resource effectiveness. This is in sharp contrast to the traditional quantum reservoir computing schemes where either the required size of the quantum reservoir or the temporal resolution in the measurement tend to be exponentially large ($\sim d^2$). In either situations, these traditional schemes are exponentially quantum resource consuming.

C. Training

To estimate the expectation value $\text{Tr}(\mathcal{O}\sigma)$, the QRPE scheme essentially maps the input state σ to a vector of probabilities for observing each readout operator

$$\sigma \xrightarrow{\text{QRP}} \bar{X} = [\langle \hat{o}_1 \rangle; \langle \hat{o}_2 \rangle; \dots; \langle \hat{o}_{N_{\text{read}}} \rangle], \quad (6)$$

and the target observable \mathcal{O} to a vector of weights

$$\mathcal{O} \xrightarrow{\text{QRP}} W = [w_1, w_2, \dots, w_{N_{\text{read}}}], \quad (7)$$

satisfying

$$W \cdot \bar{X} = \text{Tr}(\mathcal{O}\sigma). \quad (8)$$

We note that similar maps have also been studied in the context of analog quantum simulation [14, 15]. Here each readout in experiments requires only linear classical storage with respect to the system size, owing to the tensor product structure in Eq. (3). The relation given by Eq. (6) is achieved by sampling from i.i.d. copies of the n -qubit state σ and processing the reservoir readouts with statistical methods, as addressed in Sec. IID, while Eq. (7) is achieved by a training process described below.

For training, we require a one-time estimation of a known set of training states $\{|\varphi_k\rangle\}$. Here we consider the training data to be accurate, and present results that account for statistical noise occurring outside of the training phase. The reservoir dynamics are initialized by setting the parameters J , $P_{1,2}$, $E_{1,2}$ and the evolution time t . Each training step starts with an initial state of the reservoir $\rho(0) = |\varphi_k\rangle\langle\varphi_k| \otimes [|0\rangle\langle 0|]_{\text{rest}}$, which then evolves to $\rho(t)$ at time t . From sufficiently many measurement results of each input training state, we estimate the expectation value $\langle \hat{o}_i(k) \rangle$. The training data is stored by arranging $\langle \hat{o}_i(k) \rangle$ into a column vector $\bar{X}_{|\varphi_k\rangle\langle\varphi_k|}$. In this way, we collect readout vectors $\bar{X}_{|\varphi_k\rangle\langle\varphi_k|}$ corresponding to all the training states $|\varphi_k\rangle$ for $k = 1, 2, \dots, N_{\text{train}}$.

Until this step, the whole procedure is completely independent of the parameter to be estimated. The knowledge of \mathcal{O} is only required at the post processing level, where we set the target output

$$Y_k^{\text{tar}} = \langle \varphi_k | \mathcal{O} | \varphi_k \rangle. \quad (9)$$

Let $Y_k^{\text{out}} = W \cdot \bar{X}_{|\varphi_k\rangle\langle\varphi_k|}$, and the sum of squared deviations between Y_k^{out} and Y_k^{tar} is

$$\mathcal{E}_{\text{train}} = |Y^{\text{out}} - Y^{\text{tar}}|^2, \quad (10)$$

where Y^{out} is a row vector with elements Y_k^{out} , $k = 1, 2, \dots, N_{\text{train}}$, and Y^{tar} is defined similarly. For typical quantum reservoirs, a total of d^2 training states are needed to estimate arbitrary parameters for an input state supported on \mathcal{H}_d . The set of training states $\{|\varphi_k\rangle\langle\varphi_k|\}$ is a set of d^2 vectors which spans a d^2 -dimensional Hilbert space, i.e., forms an informationally complete POVM. We choose the training states

as

$$|\varphi_k\rangle = \otimes_{m=1}^n |k_m\rangle, \quad k = \sum_{m=1}^n 4^{m-1} k_m. \quad (11)$$

where $k_m \in \{0, 1, 2, 3\}$, $|0\rangle = [1; 0]$, $|1\rangle = [0; 1]$, $|2\rangle = (|0\rangle + |1\rangle)/\sqrt{2}$ and $|3\rangle = (|0\rangle + i|1\rangle)/\sqrt{2}$. Denote

$$\mathcal{T} = \mathbf{X}_t \mathbf{M}_t^{-1}, \quad (12)$$

where $\mathbf{M}_t = [|\varrho_1\rangle\langle\varrho_1|, |\varrho_2\rangle\langle\varrho_2|, \dots, |\varrho_d\rangle\langle\varrho_d|]$, $\varrho_k = |\varphi_k\rangle\langle\varphi_k|$ is the density matrix of the k -th training state, $|\cdot\rangle\langle\cdot|$ is the Louville superoperator representation, and the matrix of training data is $\mathbf{X}_t = [\bar{X}_{|\varphi_1\rangle\langle\varphi_1|}, \bar{X}_{|\varphi_2\rangle\langle\varphi_2|}, \dots]$. Then the expectation of reservoir readout for an input state σ is

$$\bar{X}_\sigma = \mathcal{T}|\sigma\rangle, \quad (13)$$

as is explained in Appendix. A. If \mathbf{X}_t is full rank, there exists a weight vector W that minimizes $\mathcal{E}_{\text{train}}$, i.e.,

$$W = Y^{\text{tar}} \mathbf{X}_t^{-1}, \quad (14)$$

which can be written as $W = \langle\langle \mathcal{O} | \mathcal{T}^{-1} \rangle\rangle$.

Leveraging pair-wise reservoir dynamics in Eq. (1) lifts the burden on training, given that the training data inherits a tensor product structure. Once the training data of a single pair of interacting reservoir nodes is collected as \mathbf{X}_p , then we have

$$\mathbf{X}_t = \bigotimes_{i=1}^n \mathbf{X}_p, \quad (15)$$

where n is the number of node pairs. Also,

$$\mathbf{M}_t = \bigotimes_{i=1}^n \mathbf{M}_p, \quad \mathcal{T} = \bigotimes_{i=1}^n \mathcal{T}_p, \quad (16)$$

where $\mathcal{T}_p = \mathbf{X}_p \mathbf{M}_p^{-1}$. Thus, the training task is effectively reduced to that of a two-node reservoir, and the full-rank requirement of \mathbf{X}_t is correspondingly reduced to that of \mathbf{X}_p . Moreover, the vector of weights only necessitates polynomial storage if the parameter \mathcal{O} can be decomposed into a finite sum of tensor products. See Appendix. A for more details.

D. Reservoir estimator

In this section we introduce the reservoir estimator for linear functions. With the training data at our disposal, we could analyze the sample efficiency of the reservoir estimators.

Suppose the observed readout operator for the i -th input copy is \hat{o}_j , then the so-called single snapshot X_i is a vector where the j -th element is 1 and the other elements are 0. For a total of N_{sample} input copies, one obtains a set of snapshots $\{X_i | i = 1, 2, \dots, N_{\text{sample}}\}$. The single-snapshot estimator is

$$\hat{\Omega} \equiv W \cdot \hat{X}, \quad (17)$$

where \hat{X} is a random variable that conforms to the probability distribution behind X_i . Eq. (8) indicates that $\hat{\Omega}$ is an unbiased estimator for $\text{Tr}(\mathcal{O}\sigma)$. Hence in data processing, we could apply the median of means (MoM) method to neutralize the effect of outliers [4, 40]. After processing $N_{\text{sample}} = KN$ input copies, we divide the snapshots into K equally sized subsets $\{X_i^v | i = 1, 2, \dots, N\}$, and compute the mean value of the single-snapshot estimators for each subset. The corresponding estimators are

$$\hat{\Omega}_M^v = \frac{1}{N} \sum_{i=1}^N W \cdot \hat{X}_i^v, \quad v = 1, 2, \dots, K. \quad (18)$$

Then, the MoM estimator is given by

$$\hat{\Omega}_{\text{MoM}} = \text{Median}\{\hat{\Omega}_M^v\}. \quad (19)$$

With this, we have

Theorem 1. *The number of quantum state inputs needed for estimating a set of M parameters $\{\mathcal{O}_i | i = 1, 2, \dots, M\}$ to precision ϵ and confidence level $1 - \delta$ scales in*

$$N_{\text{sample}} \sim O\left(\ln\left(\frac{2M}{\delta}\right) \frac{\max_i F_{\text{res}}^i}{\epsilon^2}\right). \quad (20)$$

The factor $F_{\text{res}}^i = \|\mathcal{B}_i\|_\infty$ is the variance upper bound of the single-snapshot estimator of \mathcal{O}_i maximized over the possible quantum state inputs, where $\|\cdot\|_\infty$ represents the spectral norm, and \mathcal{B}_i is defined by

$$\langle\langle \mathcal{B}_i | \mathcal{T}^{-1} \rangle\rangle = \langle\langle \mathcal{O}_i | \mathcal{T}^{-1} \rangle\rangle \odot \langle\langle \mathcal{O}_i | \mathcal{T}^{-1} \rangle\rangle. \quad (21)$$

Proof. This efficiency scaling results from the median of means method, and we consider the worst-case scenario by maximizing F_{res}^i over the set of observables. A more detailed proof is included in Appendix B. \square

The variance of a single-snapshot estimator for \mathcal{O} is invariant for parameters $\{\mathcal{O}' | \mathcal{O}' = \mathcal{O} + c\mathbb{1}, c \in \mathbb{C}\}$. Thus, one could use only the traceless part of \mathcal{O} to compute the worst-case variance upper bound. It is interesting to note that the MoM estimator won't have a visible significance in some tested cases [41, 42], where it could be replaced with the sample mean estimator.

To further analyze the sample efficiency scaling of the QRPE scheme, we have:

Theorem 2. *For a k -local parameter, e.g.*

$$\mathcal{O} = \bigotimes_{i=1}^k \mathcal{O}_i \bigotimes_{i=k+1}^n \mathbb{1}_i, \quad (22)$$

the worst-case variance upper bound $\|\mathcal{B}\|_\infty$ is the product of that of each local parameters \mathcal{O}_i , i.e.,

$$\|\mathcal{B}\|_\infty = \prod_{i=1}^k \|\mathcal{B}_i\|_\infty, \quad (23)$$

where \mathcal{B}_i satisfies

$$\langle\langle \mathcal{B}_i | \mathcal{T}_p^{-1} \rangle\rangle = \langle\langle \mathcal{O}_i | \mathcal{T}_p^{-1} \rangle\rangle \odot \langle\langle \mathcal{O}_i | \mathcal{T}_p^{-1} \rangle\rangle. \quad (24)$$

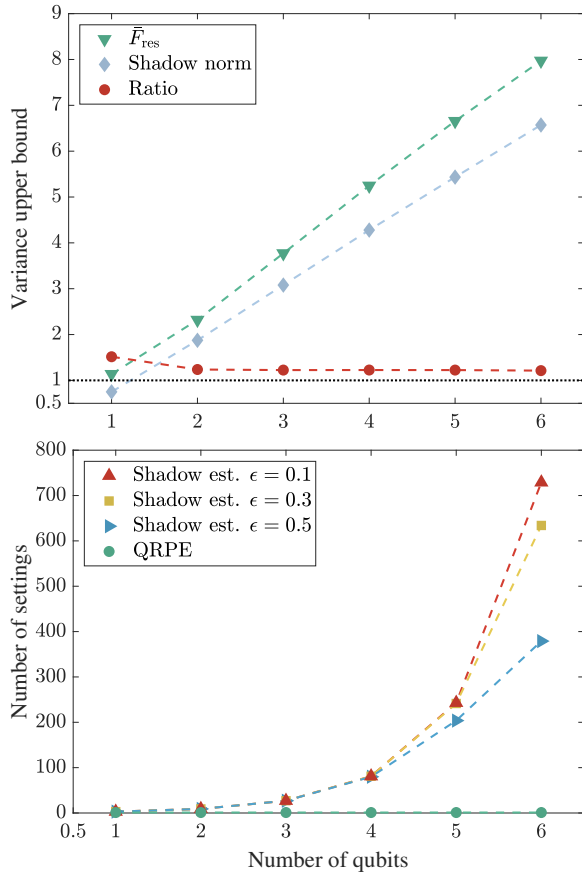


FIG. 2. Comparison with the shadow estimation with Pauli measurements [4]. (top) Average variance upper bound of fidelity estimation. For each system size we randomly generate 1000 pure states as the target states. The ratio of the average variance upper bounds for QRPE and shadow estimation remains almost constant as the number of qubits grows. (bottom) The average number of measurement settings invoked to reach a given precision with confidence level 0.90. For shadow estimation, we assume the variance in single-snapshot estimator equals a tenth of the shadow norm on the top figure. While QRPE requires only a single setting, the standard shadow protocol with Pauli measurements [4, 43] requires exponentially increasing settings to reach an arbitrary precision. The reservoir setting we choose for qubit system is given by $J = -0.41$, $P_1 = 4.0$, $P_2 = 1.3$, $E_1 = 0.71$, $E_2 = 0.46$ and $t = 1$. The unit for the Plank's constant is $\text{meV}\cdot\text{ps}$.

Proof. This theorem results from the pair-wise reservoir dynamics. See Appendix B for the details. \square

Theorem 2 indicates that for k -local parameter estimation, if a reservoir setting works well in the single-qubit case, then it also works well in the multi-qubit case. Thus, our approach for evaluating the reservoir parameters J , $P_{1,2}$, and $E_{1,2}$ is based on the performance in the single-qubit state overlap estimation task. To see why overlap estimation reflects the overall performance of observable estimation, note that the single-snapshot estimator's variance of an arbitrary parameter \mathcal{O}' satisfying $\mathcal{O}' = c_1\sigma + c_2\mathbb{1}$ equals c_1^2 times that of σ , where $c_{1,2}$ are real numbers and σ is

a density matrix. We find several settings that lead to small average variance upper bound of random target states, and choose one of them as the reservoir setting used in this manuscript. In the task of fidelity estimation, the efficiency of the current reservoir estimator outperforms the shadow estimation based on Pauli group only in a fraction of target pure states. Also, the ratio of the average variance upper bound of shadow estimation and that of the QRPE scheme is slightly larger than unity and almost invariant with the system size. While the average efficiency of the current setting only marginally differ from that of the shadow estimation, the number of settings for the standard shadow estimation is exponentially large compared to that of the present scheme. These results are shown in Fig. 2. We note that the random measurement protocol with Clifford group could obtain a scaling independent of the system size, but requires to implement complex Clifford compiling [44, 45].

Also, we could utilize random settings by probabilistic time multiplexing (PTM), where the pair-wise training data $\mathbf{X}_p(t_k)$ are collected at N_{time} different time points $\{t_k | k = 1, 2, \dots, N_{\text{time}}\}$, and the single-snapshot estimator is constructed by measuring reservoir nodes at time t_k with probability p_k , where $\sum_k p_k = 1$. The optimization over probability distributions aims to reduce the average variance upper bound of single-qubit state overlap estimation, see Appendix B for more details.

The QRPE protocol for linear functions is as follows:

1. Perform a one-time estimation of the training states of a two-node reservoir and load the training data $\{\mathbf{X}_p\}$ to classical memory.
2. Given parameters $\{\mathcal{O}_i\}$, calculate weights $\{W_i\}$ with the training data. Obtain the worst-case variance upper bound $\max_i \|\mathcal{B}_i\|_\infty$. Calculate N_{sample} with the given confidence $1 - \delta$ and additive error ϵ .
3. Process i.i.d. copies of the unknown state σ with the quantum reservoir network. Load N_{sample} snapshots $\{X_i\}$ to classical memory.
4. Calculate the estimated values $\{\tilde{\mathcal{O}}_i\}$ with the weights and snapshots.

The reservoir estimators for nonlinear functions are based on U-statistics [4, 46], which is a generalization of the sample mean estimator. It is worth noting that the reservoir snapshots are ready to be used to estimate future parameters of the input state σ .

III. APPLICATIONS

Here we provide a wide range of applications of the quantum reservoir scheme. The reservoir initialization and evolution time are fixed for all applications. See Fig. 2 for the details of reservoir settings.

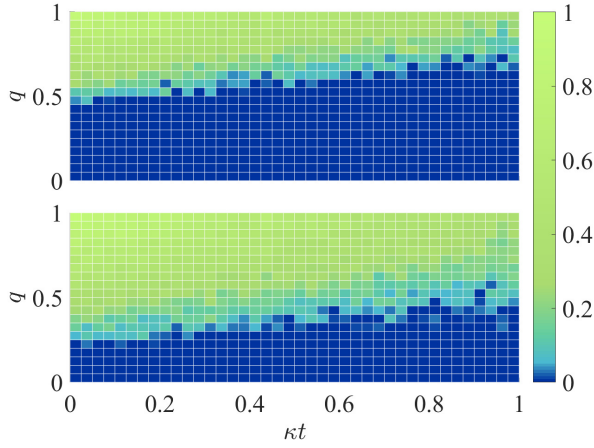


FIG. 3. Observation of entanglement sudden death. (top): estimation of W_{GME} . (bottom): estimation of W_{ME} . We use 6000 measurements for each $\{q, \kappa t\}$, and the maximal estimation error for estimating GME and ME witnesses are 0.11 and 0.13 respectively.

A. Fidelity estimation

In contrast to full quantum tomography, extracting partial information from the quantum system is more resource efficient. A particularly important feature is the degree to which a given system differs from the target system. Accordingly, quantum fidelity is a widely used distance measure of quantum states, which is a linear function of the given state when the target state is a pure state [47, 48]. Here we present an illustrative example of how the reservoir estimation scheme works in random pure state fidelity estimation. Numerical results indicate that the average worst-case variance upper bound for QRPE is close to that of random Pauli measurements, as shown in Fig. 2.

B. Entanglement detection

Entanglement is an indispensable resource in tasks ranging from quantum computation to quantum communication [49]. Whether one can claim its existence for a given system has aroused both theoretical and experimental interests [50–54]. However, the difficulty in describing the convex space of separable states poses a trade-off relation between the detection ability and effectiveness of entanglement criteria [55]. With its capability of estimating multiple observables simultaneously, the reservoir estimation scheme is a natural fit for the task of entanglement detection with linear entanglement criteria.

We illustrate the QRPE scheme on the detection of an intriguing and more targeted phenomenon, the entanglement sudden death [56, 57]. Consider a three-qubit GHZ-type state [58]

$$\rho = \frac{1-q}{8}\mathbb{1} + q\rho_{\text{G}}, \quad (25)$$

where $\rho_{\text{G}} = (|000\rangle + |111\rangle)(\langle 000| + \langle 111|)/2$. The dephasing channel is defined by the Kraus operators

$$K_0 = \sqrt{1-p}\mathbb{1}, \quad K_{1,2} = \frac{\sqrt{p}}{2}(\mathbb{1} \pm \zeta^z). \quad (26)$$

Set $p = 1 - \exp(-\kappa t)$, then dephasing of the initial state ρ reflects on a factor $\exp(-\kappa t)$ that times the off-diagonal elements. We use the following optimal linear entanglement witnesses for detecting genuine multipartite entanglement (GME) and any multipartite entanglement (ME) respectively [59]:

$$\begin{aligned} W_{\text{GME}} &= \mathbb{1} - 2\rho_{\text{G}}, \\ W_{\text{ME}} &= \mathbb{1} - 4\rho_{\text{G}} + 2\rho_{\text{G}-}. \end{aligned} \quad (27)$$

where $\rho_{\text{G}-} = (|000\rangle - |111\rangle)(\langle 000| - \langle 111|)/2$. We normalize the spectral norm of the two witnesses, and estimate them simultaneously. With a total of 6000 snapshots for each $\{q, \kappa t\}$, we illustrate the results in Fig. 3.

C. Estimating expectation values of local and global observables

Estimating the values of observables is a fundamental task in various quantum information processing tasks. For local observables, we present the numerical results of estimating the local Pauli observables for random four-qubit states. We observe an exponential growth in sample complexity with the locality in Pauli observable estimation, which is in line with Theorem 2. The numerical result is shown in Fig. 4.

For global observables, we consider the task of GHZ state fidelity estimation. For an input GHZ state with three, six, nine and twelve qubits, we present the results of numerical experiment as the number of input copies versus the average error in Fig. 5.

D. Estimating nonlinear functions

The reservoir measurements only describe linear functions in Eq. (8). Nevertheless, experimentally accessible nonlinear parameters are typically measured by estimating linear functions that can be translated into the QRPE scheme. For instance, the SWAP trick is widely used in purity estimation. For two copies of the input state σ , the SWAP operator obeys $\text{Tr}(S\sigma \otimes \sigma) = \text{Tr}(\sigma^2)$. Numerical simulation of the purity estimation of 10000 random one-qubit input states shows that the average variance upper bound is around 2.9.

The Rényi entropy is another important nonlinear factor for characterizing entanglement, which is the logarithm of subsystem purity. The estimator of second Rényi entropy is

$$\text{Tr}(\rho_A^2) = \text{Tr}(S_A \rho \otimes \rho), \quad (28)$$

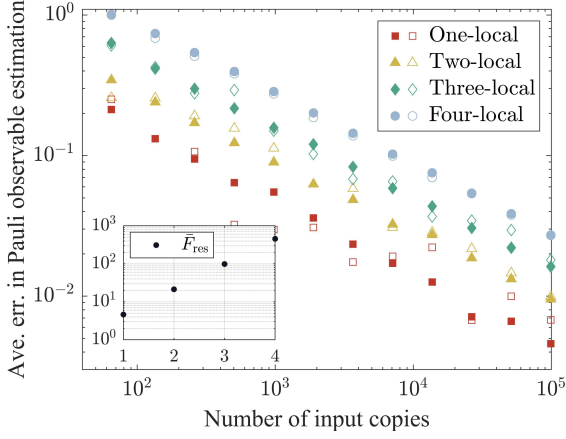


FIG. 4. Numerical experiment for estimating Pauli observables for random one, two, three and four-qubit input states. Each data point represents the average error of all the k -local Pauli observables of a random k -qubit input state. The solid marks represents the average performance of 30 independent experiments, while the hollow marks represents a single experiment. The subfigure shows the variance upper bound \bar{F}_{res} , averaged over the k -local Pauli observables. Numerical results indicate that the worst-case sample complexity of estimating Pauli observables increases exponentially with the locality.

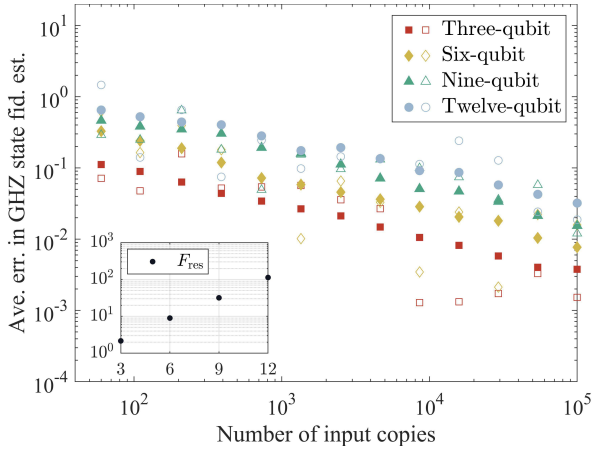


FIG. 5. Numerical experiment for identifying GHZ states with fidelity estimation. The solid marks represents the average performance of 50 independent experiments, while the hollow marks represents a single experiment. The subfigure shows the variance upper bound for the k -qubit GHZ state. Numerical results indicate that the sample complexity of identifying GHZ states increases exponentially with the number of qubits.

where S_A is the SWAP operator acting on subsystem A of two copies of ρ . The second Rényi entropy of small subsystems is useful in avoiding weak barren plateaus (WBP) [60]. Here we perform WBP diagnosis with the reservoir estimation scheme. For an initial state $|0\rangle^{\otimes 14}$, each gate sequence of the variational quantum eigensolver (VQE) circuit is composed of random local rotations $\exp(-\frac{i}{2}\theta\varsigma)$, where $\theta \in [\pi/20, \pi/20]$ and $\varsigma \in \{\varsigma_x, \varsigma_y, \varsigma_z\}$, and nearest-neighbor controlled-Z

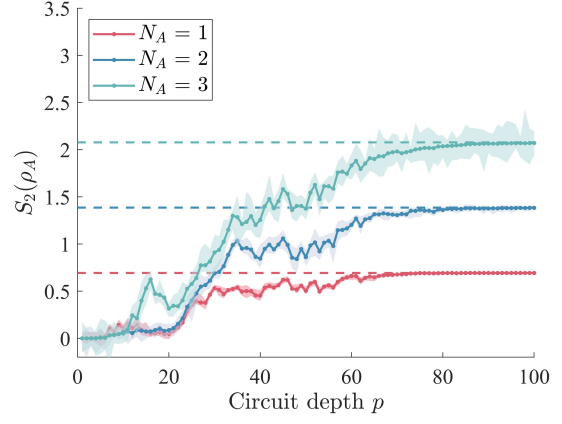


FIG. 6. Saturation of the second Rényi entropy $S_2(\rho_A)$ of a small region A consisting of N_A qubits. The solid curves represent $S_2(\rho_A)$ of a fourteen-qubit state generated by a VQE circuit with depth p , which approaches the page entropy represented by the dashed line. For reservoir estimation at each circuit depth we use 2000 independent snapshots. The shaded region is the fluctuation of estimated value in 10 independent estimations.

gates with periodic condition. We detect the emergence of WBP by estimating the second Rényi entropy of a small region consisting of N_A qubits via 2000 measurements at each circuit depth. The numerical experiment is shown in Fig. 6.

IV. HIGHER-DIMENSIONAL AND HYBRID SYSTEMS

Higher-dimensional systems and hybrid systems with non-identical local dimensions are of fundamental importance as a playground to reveal intriguing quantum phenomena, such as quantum steering [61, 62] and the demonstration of contextuality and nonlocality trade-off [63, 64]. Here we demonstrate the flexibility of our scheme beyond the qubit systems.

The bosonic Hamiltonian for the qudit reservoir network is given by

$$\begin{aligned} \hat{H} = & \sum_{\langle i,j \rangle} J(\hat{a}_i^\dagger \hat{a}_j + \hat{a}_j^\dagger \hat{a}_i) + P_1(\hat{a}_i^\dagger + \hat{a}_i) \\ & + P_2(\hat{a}_j^\dagger + \hat{a}_j) + E_1 \hat{a}_i^\dagger \hat{a}_i + E_2 \hat{a}_j^\dagger \hat{a}_j \\ & + \alpha_1 \hat{a}_i^\dagger \hat{a}_i^\dagger \hat{a}_i \hat{a}_i + \alpha_2 \hat{a}_j^\dagger \hat{a}_j^\dagger \hat{a}_j \hat{a}_j, \end{aligned} \quad (29)$$

where the operators \hat{a} represent lowering operators of the quantum nodes (qudits). The parameters J , $P_{1,2}$, $E_{1,2}$ and $\alpha_{1,2}$ represent hopping, onsite driving field, energy and nonlinear strength respectively. We consider the unitary time evolution governed by the quantum Liouville equation.

For qudit systems with local dimension d , a superoperator basis consists of the generalized Gell-Mann matrices and the normalized identity [65]. The readout

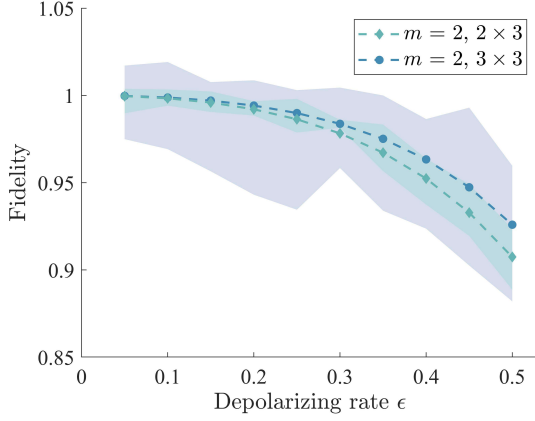


FIG. 7. The virtual distillation of maximally entangled states mixed with depolarizing noise in 2×3 and 3×3 dimensional systems. The solid curves represent the fidelity of the distilled state with $m = 2$. The shaded region is the range of fluctuation of the estimated value in 10 independent estimations. For each reservoir estimation we use 10000 independent measurement readouts. The reservoir setting we choose for qutrit systems is $J = 0.9$, $P_1 = 2.1$, $P_2 = 1.1$, $E_1 = 1.1$, $E_2 = 0.4$, $\alpha_1 = 0.6$, $\alpha_2 = 0.7$.

operators are constructed in the same way with that of the qubit system, the only difference is that there are d projection operators instead of two, corresponding to the d possible population numbers. Due to the tensor product structure of the measurements and training states, the reservoir estimation scheme can be naturally extended to hybrid systems with non-identical local dimensions, such as qubit-qutrit systems. The pair-wise reservoir setting for a pair of qudit nodes is the same with that of qudit reservoirs.

For application we apply virtual distillation (VD) [66–68] to estimate the fidelity of a noisy state ρ_ϵ ,

$$\langle |\psi\rangle\langle\psi| \rangle_{\text{VD}} = \frac{\text{Tr}(\rho_\epsilon^m |\psi\rangle\langle\psi|)}{\text{Tr}(\rho_\epsilon^m)}, \quad (30)$$

where

$$\rho_\epsilon = (1 - \epsilon)|\psi\rangle\langle\psi| + \epsilon\mathbb{1}. \quad (31)$$

The estimator for ρ_ϵ^m is chosen as

$$\frac{1}{P(N, m)} \sum_{i=1}^* \prod_{s_i=1}^m \hat{\rho}_{s_i}, \quad (32)$$

where $\hat{\rho}_{s_i}$ is the single-snapshot estimator of the noisy state ρ_ϵ , $P(N, m)$ is the m -permutations of N , \sum^* denotes the summation over all distinct subscripts, i.e., s_1, s_2, \dots, s_m is a m -tuple of indices from the set $\{1, \dots, N\}$ with distinct entries. The denominator is estimated similarly. The estimation results are shown in Fig. 7 for the following maximally entangled qubit-qutrit and two-qutrit pairs,

$$\begin{aligned} |\psi_1\rangle &= \frac{1}{2}(|10\rangle + |12\rangle) + \frac{1}{\sqrt{2}}|01\rangle, \\ |\psi_2\rangle &= \frac{1}{\sqrt{3}}(|00\rangle + |11\rangle + |22\rangle). \end{aligned} \quad (33)$$

V. CONCLUSION

We have presented a direct parameter estimation scheme, where a classical representation of quantum states is constructed with quantum reservoir networks and used for parameter estimation in the post-processing phase. Unlike existing techniques of shadow estimation that considers complex unitary ensembles or randomized measurements, our scheme explores the versatility of the quantum reservoir platform and requires only a single measurement setting. For the reservoir network, the pair-wise interacting reservoir nodes considered in our scheme results in minimal quantum hardware and training resources. The sample complexity has been rarely addressed in previous works on quantum reservoir computing. In contrast, we have established a stringent performance guarantee regarding the number of samples to be processed by the reservoir network, which is independent of the input quantum state. Furthermore, our scheme can be naturally extended to higher-dimensional systems and hybrid systems with non-identical local dimensions. We complement the theoretical results with diverse applications.

For future research, reservoir computing is suitable for temporal pattern recognition, classification, and generation [34, 69, 70]. While we have proposed a criteria for analyzing the statistical fluctuation of quantum reservoir outputs in parameter estimation, it is important to do so in temporal information processing tasks such as temporal quantum tomography [71] and nonlinear temporal machine learning [72]. Also, it is important to further optimize the reservoir networks regarding the sample complexity and investigate whether the efficiency lower bound for local measurements [4] can be achieved with the quantum reservoir platform. Moreover, there has been extensive research conducted on the learning abilities of quantum reservoir networks in tasks ranging from quantum to real-world problems [73–76]. These studies explore various network topologies and connectivities. While the pair-wise quantum reservoir construction is beneficial for parameter estimation, there lacks a general understanding of the role of topology and connectivity in quantum reservoir computing regarding sample complexity. Another topic is the noise effect. There are inspiring discussions on the noisy training data [77], robustness in tomographic completeness [78] and benefits of quantum noise [79]. In our scheme the influence of time independent system noise on \mathcal{T} cancels out by a direct observation of Eq. (13). However, a complete discussion on the noise effect and its mitigation in quantum reservoir processing is important for future experiments.

ACKNOWLEDGMENTS

We are grateful to Yanwu Gu, Zihao Li, Zhenpeng Xu and Ye-Chao Liu for helpful discussions. This

work was supported by the National Natural Science Foundation of China (Grants No. 12175014 and No. 92265115) and the National Key R&D Program of China (Grant No. 2022YFA1404900). S.G. ac-

knowledges support from the Excellent Young Scientists Fund Program (Overseas) of China, and the National Natural Science Foundation of China (Grant No. 12274034).

-
- [1] J. Preskill, Quantum computing in the NISQ era and beyond, *Quantum* **2**, 79 (2018).
 - [2] S. Aaronson, Shadow tomography of quantum states, in *Proc. of the 50th ACM STOC*, STOC 2018 (ACM, 2018) p. 325–338.
 - [3] M. Painsi and A. Kalev, An approximate description of quantum states, [arXiv:1910.10543](https://arxiv.org/abs/1910.10543).
 - [4] H.-Y. Huang, R. Kueng, and J. Preskill, Predicting many properties of a quantum system from very few measurements, *Nat. Phys.* **16**, 1050 (2020).
 - [5] A. Elben, S. T. Flammia, H.-Y. Huang, R. Kueng, J. Preskill, B. Vermersch, and P. Zoller, The randomized measurement toolbox, *Nat. Rev. Phys.* **5**, 9 (2023).
 - [6] H. C. Nguyen, J. L. Bönsel, J. Steinberg, and O. Gühne, Optimizing shadow tomography with generalized measurements, *Phys. Rev. Lett.* **129**, 220502 (2022).
 - [7] D. McNulty, F. B. Maciejewski, and M. Oszmaniec, Estimating quantum Hamiltonians via joint measurements of noisy noncommuting observables, *Phys. Rev. Lett.* **130**, 100801 (2023).
 - [8] G. García-Pérez, M. A. Rossi, B. Sokolov, F. Tacchino, P. K. Barkoutsos, G. Mazzola, I. Tavernelli, and S. Maniscalco, Learning to measure: Adaptive informationally complete generalized measurements for quantum algorithms, *PRX Quantum* **2**, 040342 (2021).
 - [9] A. Elben, R. Kueng, H.-Y. R. Huang, R. van Bijnen, C. Kokail, M. Dalmonte, P. Calabrese, B. Kraus, J. Preskill, P. Zoller, and B. Vermersch, Mixed-state entanglement from local randomized measurements, *Phys. Rev. Lett.* **125**, 200501 (2020).
 - [10] A. Elben, J. Yu, G. Zhu, M. Hafezi, F. Pollmann, P. Zoller, and B. Vermersch, Many-body topological invariants from randomized measurements in synthetic quantum matter, *Sci. Adv.* **6**, eaaz3666 (2020).
 - [11] H.-Y. Huang, R. Kueng, G. Torlai, V. V. Albert, and J. Preskill, Provably efficient machine learning for quantum many-body problems, *Science* **377**, eabk3333 (2022).
 - [12] H.-Y. Huang, R. Kueng, and J. Preskill, Efficient estimation of Pauli observables by derandomization, *Phys. Rev. Lett.* **127**, 030503 (2021).
 - [13] R. Stricker, M. Meth, L. Postler, C. Edmunds, C. Ferrie, R. Blatt, P. Schindler, T. Monz, R. Kueng, and M. Ringbauer, Experimental single-setting quantum state tomography, *PRX Quantum* **3**, 040310 (2022).
 - [14] M. C. Tran, D. K. Mark, W. W. Ho, and S. Choi, Measuring arbitrary physical properties in analog quantum simulation, *Phys. Rev. X* **13**, 011049 (2023).
 - [15] M. McGinley and M. Fava, Shadow tomography from emergent state designs in analog quantum simulators (2022), [arXiv:2212.02543](https://arxiv.org/abs/2212.02543) [quant-ph].
 - [16] H. Zhu, Multiqubit Clifford groups are unitary 3-designs, *Phys. Rev. A* **96**, 062336 (2017).
 - [17] A. Elben, B. Vermersch, C. F. Roos, and P. Zoller, Statistical correlations between locally randomized measurements: A toolbox for probing entanglement in many-body quantum states, *Phys. Rev. A* **99**, 052323 (2019).
 - [18] H.-Y. Hu and Y.-Z. You, Hamiltonian-driven shadow tomography of quantum states, *Phys. Rev. Res.* **4**, 013054 (2022).
 - [19] H.-Y. Hu, S. Choi, and Y.-Z. You, Classical shadow tomography with locally scrambled quantum dynamics, *Phys. Rev. Res.* **5**, 023027 (2023).
 - [20] D. Grier, H. Pashayan, and L. Schaeffer, Sample-optimal classical shadows for pure states, [arXiv:2211.11810](https://arxiv.org/abs/2211.11810).
 - [21] M. Schuld, I. Sinayskiy, and F. Petruccione, The quest for a quantum neural network, *Quantum Inf. Process.* **13**, 2567 (2014).
 - [22] J. Biamonte, P. Wittek, N. Pancotti, P. Rebentrost, N. Wiebe, and S. Lloyd, Quantum machine learning, *Nature* **549**, 195 (2017).
 - [23] M. Schuld and F. Petruccione, *Machine learning with quantum computers* (Springer, 2021).
 - [24] V. Havlíček, A. D. Córcoles, K. Temme, A. W. Harrow, A. Kandala, J. M. Chow, and J. M. Gambetta, Supervised learning with quantum-enhanced feature spaces, *Nature* **567**, 209 (2019).
 - [25] A. Abbas, D. Sutter, C. Zoufal, A. Lucchi, A. Figalli, and S. Woerner, The power of quantum neural networks, *Nat. Comput. Sci.* **1**, 403 (2021).
 - [26] A. K. Jain, J. Mao, and K. M. Mohiuddin, Artificial neural networks: A tutorial, *Computer* **29**, 31 (1996).
 - [27] M. Cerezo, G. Verdon, H.-Y. Huang, L. Cincio, and P. J. Coles, Challenges and opportunities in quantum machine learning, *Nat. Comput. Sci.* **2**, 567 (2022).
 - [28] J. R. McClean, S. Boixo, V. N. Smelyanskiy, R. Babush, and H. Neven, Barren plateaus in quantum neural network training landscapes, *Nat. Commun.* **9**, 4812 (2018).
 - [29] M. Cerezo, A. Sone, T. Volkoff, L. Cincio, and P. J. Coles, Cost function dependent barren plateaus in shallow parametrized quantum circuits, *Nat. Commun.* **12**, 1791 (2021).
 - [30] L. Bittel and M. Kliesch, Training variational quantum algorithms is NP-hard, *Phys. Rev. Lett.* **127**, 120502 (2021).
 - [31] S. Wang, E. Fontana, M. Cerezo, K. Sharma, A. Sone, L. Cincio, and P. J. Coles, Noise-induced barren plateaus in variational quantum algorithms, *Nat. Commun.* **12**, 6961 (2021).
 - [32] S. Ghosh, A. Opala, M. Matuszewski, T. Paterek, and T. C. H. Liew, Quantum reservoir processing, *npj Quantum Inf.* **5**, 35 (2019).
 - [33] S. Ghosh, T. Paterek, and T. C. H. Liew, Quantum neuromorphic platform for quantum state preparation, *Phys. Rev. Lett.* **123**, 260404 (2019).
 - [34] K. Nakajima, Physical reservoir computing—an introductory perspective, *Jpn. J. Appl. Phys.* **59**, 060501 (2020).
 - [35] J. Majer, J. Chow, J. Gambetta, J. Koch, B. Johnson, J. Schreier, L. Frunzio, D. Schuster, A. A. Houck,

- A. Wallraff, *et al.*, Coupling superconducting qubits via a cavity bus, *Nature* **449**, 443 (2007).
- [36] G. A. Álvarez, D. Suter, and R. Kaiser, Localization-delocalization transition in the dynamics of dipolar-coupled nuclear spins, *Science* **349**, 846 (2015).
- [37] T. Kusumoto, K. Mitarai, K. Fujii, M. Kitagawa, and M. Negoro, Experimental quantum kernel trick with nuclear spins in a solid, *npj Quantum Inf.* **7**, 94 (2021).
- [38] Y. P. Kandel, H. Qiao, S. Fallahi, G. C. Gardner, M. J. Manfra, and J. M. Nichol, Adiabatic quantum state transfer in a semiconductor quantum-dot spin chain, *Nat. Commun.* **12**, 1 (2021).
- [39] D. Porras and J. I. Cirac, Effective quantum spin systems with trapped ions, *Phys. Rev. Lett.* **92**, 207901 (2004).
- [40] S. Chen, W. Yu, P. Zeng, and S. T. Flammia, Robust shadow estimation, *PRX Quantum* **2**, 030348 (2021).
- [41] A. Acharya, S. Saha, and A. M. Sengupta, Shadow tomography based on informationally complete positive operator-valued measure, *Phys. Rev. A* **104**, 052418 (2021).
- [42] G. Struchalin, Y. A. Zagorovskii, E. Kovlakov, S. Straupe, and S. Kulik, Experimental estimation of quantum state properties from classical shadows, *PRX Quantum* **2**, 010307 (2021).
- [43] C. Hadfield, S. Bravyi, R. Raymond, and A. Mezza-capo, Measurements of quantum Hamiltonians with locally-biased classical shadows, *Commun. Math. Phys.* **391**, 951 (2022).
- [44] T. J. Proctor, A. Carignan-Dugas, K. Rudinger, E. Nielsen, R. Blume-Kohout, and K. Young, Direct randomized benchmarking for multiqubit devices, *Phys. Rev. Lett.* **123**, 030503 (2019).
- [45] C. Bertoni, J. Haferkamp, M. Hinsche, M. Ioannou, J. Eisert, and H. Pashayan, Shallow shadows: Expectation estimation using low-depth random Clifford circuits, *arXiv:2209.12924*.
- [46] W. Hoeffding, A class of statistics with asymptotically normal distribution, *Ann. Math. Statist.* **19**, 293 (1948).
- [47] S. T. Flammia and Y.-K. Liu, Direct fidelity estimation from few Pauli measurements, *Phys. Rev. Lett.* **106**, 230501 (2011).
- [48] M. Cerezo, A. Poremba, L. Cincio, and P. J. Coles, Variational quantum fidelity estimation, *Quantum* **4**, 248 (2020).
- [49] V. Vedral, Quantum entanglement, *Nat. Phys.* **10**, 256 (2014).
- [50] O. Gühne, C.-Y. Lu, W.-B. Gao, and J.-W. Pan, Toolbox for entanglement detection and fidelity estimation, *Phys. Rev. A* **76**, 030305 (2007).
- [51] O. Gühne and G. Tóth, Entanglement detection, *Phys. Rep.* **474**, 1 (2009).
- [52] A. Dimić and B. Dakić, Single-copy entanglement detection, *npj Quantum Inf.* **4**, 11 (2018).
- [53] C. Spengler, M. Huber, S. Brierley, T. Adaktylos, and B. C. Hiesmayr, Entanglement detection via mutually unbiased bases, *Phys. Rev. A* **86**, 022311 (2012).
- [54] G. Tóth and O. Gühne, Entanglement detection in the stabilizer formalism, *Phys. Rev. A* **72**, 022340 (2005).
- [55] P. Liu, Z. Liu, S. Chen, and X. Ma, Fundamental limitation on the detectability of entanglement, *Phys. Rev. Lett.* **129**, 230503 (2022).
- [56] T. Yu and J. H. Eberly, Sudden death of entanglement, *Science* **323**, 598 (2009).
- [57] M. P. Almeida, F. de Melo, M. Hor-Meyll, A. Salles, S. P. Walborn, P. H. S. Ribeiro, and L. Davidovich, Environment-induced sudden death of entanglement, *Science* **316**, 579 (2007).
- [58] Y. S. Weinstein, Tripartite entanglement witnesses and entanglement sudden death, *Phys. Rev. A* **79**, 012318 (2009).
- [59] C. Eltschka and J. Siewert, Optimal witnesses for three-qubit entanglement from Greenberger-Horne-Zeilinger symmetry, *Quantum Inf. Comput.* **13**, 210 (2013).
- [60] S. H. Sack, R. A. Medina, A. A. Michailidis, R. Kueng, and M. Serbyn, Avoiding barren plateaus using classical shadows, *PRX Quantum* **3**, 020365 (2022).
- [61] R. Uola, A. C. S. Costa, H. C. Nguyen, and O. Gühne, Quantum steering, *Rev. Mod. Phys.* **92**, 015001 (2020).
- [62] M. T. Quintino, N. Brunner, and M. Huber, Superactivation of quantum steering, *Phys. Rev. A* **94**, 062123 (2016).
- [63] P. Kurzyński, A. Cabello, and D. Kaszlikowski, Fundamental monogamy relation between contextuality and nonlocality, *Phys. Rev. Lett.* **112**, 100401 (2014).
- [64] X. Zhan, X. Zhang, J. Li, Y. Zhang, B. C. Sanders, and P. Xue, Realization of the contextuality-nonlocality tradeoff with a qubit-qutrit photon pair, *Phys. Rev. Lett.* **116**, 090401 (2016).
- [65] M. Gell-Mann, Symmetries of baryons and mesons, *Phys. Rev.* **125**, 1067 (1962).
- [66] W. J. Huggins, S. McArdle, T. E. O'Brien, J. Lee, N. C. Rubin, S. Boixo, K. B. Whaley, R. Babbush, and J. R. McClean, Virtual distillation for quantum error mitigation, *Phys. Rev. X* **11**, 041036 (2021).
- [67] H.-Y. Hu, R. LaRose, Y.-Z. You, E. Rieffel, and Z. Wang, Logical shadow tomography: Efficient estimation of error-mitigated observables, *arXiv:2203.07263*.
- [68] A. Seif, Z.-P. Cui, S. Zhou, S. Chen, and L. Jiang, Shadow distillation: Quantum error mitigation with classical shadows for near-term quantum processors, *PRX Quantum* **4**, 010303 (2023).
- [69] P. Mújal, R. Martínez-Peña, G. L. Giorgi, M. C. Soriano, and R. Zambrini, Time-series quantum reservoir computing with weak and projective measurements, *npj Quantum Inf.* **9**, 16 (2023).
- [70] G. Tanaka, T. Yamane, J. B. Héroux, R. Nakane, N. Kanazawa, S. Takeda, H. Numata, D. Nakano, and A. Hirose, Recent advances in physical reservoir computing: A review, *Neural Networks* **115**, 100 (2019).
- [71] Q. H. Tran and K. Nakajima, Learning temporal quantum tomography, *Phys. Rev. Lett.* **127**, 260401 (2021).
- [72] K. Fujii and K. Nakajima, Harnessing disordered-ensemble quantum dynamics for machine learning, *Phys. Rev. Appl.* **8**, 024030 (2017).
- [73] A. Kutvonen, K. Fujii, and T. Sagawa, Optimizing a quantum reservoir computer for time series prediction, *Sci. Rep.* **10**, 14687 (2020).
- [74] W. Xia, J. Zou, X. Qiu, and X. Li, The reservoir learning power across quantum many-body localization transition, *Front. Phys.* **17**, 33506 (2022).
- [75] W. Xia, J. Zou, X. Qiu, F. Chen, B. Zhu, C. Li, D.-L. Deng, and X. Li, Configured quantum reservoir computing for multi-task machine learning, *arXiv:2303.17629*.

- [76] R. A. Bravo, K. Najafi, X. Gao, and S. F. Yelin, Quantum reservoir computing using arrays of rydberg atoms, *PRX Quantum* **3**, 030325 (2022).
- [77] L. Innocenti, S. Lorenzo, I. Palmisano, A. Ferraro, M. Paternostro, and G. M. Palma, On the potential and limitations of quantum extreme learning machines, [arXiv:2210.00780](https://arxiv.org/abs/2210.00780).
- [78] T. Krisnanda, H. Xu, S. Ghosh, and T. C. H. Liew, Tomographic completeness and robustness of quantum reservoir networks, *Phys. Rev. A* **107**, 042402 (2023).
- [79] T. Kubota, Y. Suzuki, S. Kobayashi, Q. H. Tran, N. Yamamoto, and K. Nakajima, Temporal information processing induced by quantum noise, *Phys. Rev. Res.* **5**, 023057 (2023).
- [80] I. Bengtsson and K. Życzkowski, *Geometry of Quantum States: An Introduction to Quantum Entanglement*, 2nd ed. (Cambridge University Press, Cambridge, UK, 2017).

Appendix A: Theoretical interpretation of the QRPE scheme

We start with the qubit systems for conciseness, but our method can be naturally extended to qudit systems and hybrid systems with different local dimensions. To show how the QRPE scheme works, some may find it beneficial to examine the reservoir transformation from a geometric perspective. The weights for an arbitrary parameter \mathcal{O} and the readout probabilities for an arbitrary input state σ are represented by vectors $W_{\mathcal{O}}$ and \bar{X}_{σ} in the flat Euclidean space $\mathbf{E}^{d \times d}$, as shown in Eqs. (6) and (7) respectively. Since $\sum_{i=1}^{d^2} \langle \hat{o}_i \rangle_{\sigma} = 1$, the set $\mathcal{C} = \{\bar{X}_{\sigma} \mid \sigma \succeq 0, \text{Tr}(\sigma) = 1\}$ is a region on a $(d^2 - 1)$ -dimensional hyperplane. In addition, we have

Lemma 1. *The reservoir transformation with pair-wise reservoir dynamics is an affine map from the $(d^2 - 1)$ -dimensional state space to the $(d^2 - 1)$ -dimensional convex region \mathcal{C} .*

Proof. From Eq. (2) we have

$$\langle \hat{o}_i \rangle_{\sigma} = \text{Tr}(\hat{o}_i \rho(t)) = \text{Tr}(\langle 0 | \hat{U}(t) \hat{o}_i \hat{U}^{\dagger}(t) | 0 \rangle_{\text{rest}} \sigma) = \langle \mathcal{T}(\hat{o}_i) | \sigma \rangle, \quad (\text{A1})$$

where $\mathcal{T}(\hat{o}_i) = \langle 0 | \hat{U}(t) \hat{o}_i \hat{U}^{\dagger}(t) | 0 \rangle_{\text{rest}}$, and $|\cdot\rangle$ is the Liouville superoperator representation, i.e., to vectorize an operator by expanding it on an orthonormal operator basis. We observe that the reservoir processing is equivalent to a POVM measurement on the input state, with ancilla qubits prepared in the $|0\rangle$ state. Define the dynamics matrix

$$\mathcal{T} = [\langle \mathcal{T}(\hat{o}_1) |; \langle \mathcal{T}(\hat{o}_2) |; \dots; \langle \mathcal{T}(\hat{o}_{d^2}) |], \quad (\text{A2})$$

then for an arbitrary input state σ ,

$$\bar{X}_{\sigma} = \mathcal{T} | \sigma \rangle. \quad (\text{A3})$$

We note that for pair-wise interaction, the columns of \mathcal{T} has a tensor product structure. Since the pair-wise evolution operator for n -qubit input states satisfies $\hat{U}(t) = \bigotimes_{i=1}^n \hat{U}_{\text{p.w.}}(t)$, we have

$$\mathcal{T}(\hat{C}_S) = \langle 0 | \hat{U}(t) \hat{C}_S \hat{U}^{\dagger}(t) | 0 \rangle_{\text{rest}} = \langle 0 | \hat{U}(t) \prod_{i \in S} \frac{\mathbb{1} - \varsigma_i^z}{2} \prod_{j \notin S} \frac{\mathbb{1} + \varsigma_j^z}{2} \hat{U}^{\dagger}(t) | 0 \rangle_{\text{rest}} = \bigotimes_{i=1}^n \mathcal{T}_i(\hat{C}_S), \quad (\text{A4})$$

where

$$\mathcal{T}_i(\hat{C}_S) = \langle 0 | \hat{U}_{\text{p.w.}}(t) \mathcal{M}_i \hat{U}_{\text{p.w.}}^{\dagger}(t) | 0 \rangle \quad (\text{A5})$$

is a 2×2 matrix, \mathcal{M}_i is the two-qubit Pauli-Z projection operator acting on the pair of interacting reservoir nodes that connected to the i -th qubit of the input state, and $\langle 0 | \cdot | 0 \rangle$ acts on the reservoir node that didn't connect to the input state directly. There are only four distinct elements $\{\mathcal{T}_1, \mathcal{T}_2, \mathcal{T}_3, \mathcal{T}_4\}$ in the set $\{\mathcal{T}_i(\hat{o}_1), \dots, \mathcal{T}_i(\hat{o}_{d^2})\}$, which correspond to the four different two-qubit Pauli-Z projections $\{\mathcal{M}_i\}$. In fact,

$$\mathcal{T} = \bigotimes_{i=1}^n \mathcal{T}_{\text{p.w.}}, \quad (\text{A6})$$

where $\mathcal{T}_{\text{p.w.}}$ is the pair-wise dynamics matrix for a single qubit input state, i.e., $\mathcal{T}_{\text{p.w.}} = [\langle \mathcal{T}_1 |; \langle \mathcal{T}_2 |; \langle \mathcal{T}_3 |; \langle \mathcal{T}_4 |]$. The training process guarantees that the set of operators $\{\mathcal{T}_1, \mathcal{T}_2, \mathcal{T}_3, \mathcal{T}_4\}$ is tomographically complete, i.e., $\mathcal{T}_{\text{p.w.}}$ is invertible, then \mathcal{T} is also invertible. So the reservoir transformation is an affine map from the state space to the $(d^2 - 1)$ -dimensional region \mathcal{C} . Also, we note that Eq. (A3) indicates

$$\lambda \bar{X}_{\sigma_0} + (1 - \lambda) \bar{X}_{\sigma_1} = \bar{X}_{\lambda \sigma_0 + (1 - \lambda) \sigma_1}, \quad (\text{A7})$$

where $1 \geq \lambda \geq 0$. Since $\bar{X}_{\lambda \sigma_0 + (1 - \lambda) \sigma_1} \in \mathcal{C}$, Eq. (A7) indicates that \mathcal{C} is a convex region. \square

The basic QRPE model behind various scenarios that we consider in this work is as follows:

Theorem 3. *For an unknown state σ in a d -dimensional Hilbert space, one can linearly combine the read-out operators $\{\hat{o}_i\}$ of an $N_{\text{node}} = 2\log_2(d)$ reservoir into unbiased estimators of arbitrary parameters $\{\mathcal{O}_i\}$, if supplemented with the training data from d^2 linearly independent states.*

Proof. Firstly we note that the d^2 training points $\{\bar{X}_{|\varphi_k\rangle\langle\varphi_k|}\}$ are not confined to any $(d^2 - 2)$ -dimensional subspace, i.e., they form a $(d^2 - 1)$ -simplex [80]. Linear independence indicates that the training states in Eq. (11) form a $(d^2 - 1)$ -simplex in the state space, then Lemma 1 shows that the training points also form a $(d^2 - 1)$ -simplex in \mathcal{C} . Thus, an arbitrary d^2 -dimensional target vector Y^{tar} in Eq. (9) can be realized by taking the inner product of the training vectors $\{\bar{X}_{|\varphi_k\rangle\langle\varphi_k|}\}$ with a unique weight vector W , which is acquired in the training phase. Also, one gets

$$\bar{X}_\sigma = \sum_{k=1}^{d^2} c_k^\sigma \bar{X}_{|\varphi_k\rangle\langle\varphi_k|}, \quad (\text{A8})$$

where $\{c_k^\sigma\}$ is the set of unique barycentric coordinates for \bar{X}_σ . We have

$$W \cdot \bar{X}_\sigma = \sum_{k=1}^{d^2} c_k^\sigma W \cdot \bar{X}_{|\varphi_k\rangle\langle\varphi_k|} = \sum_{k=1}^{d^2} c_k^\sigma \text{Tr}(\mathcal{O}|\varphi_k\rangle\langle\varphi_k|) = \text{Tr}\left(\mathcal{O} \sum_{k=1}^{d^2} c_k^\sigma |\varphi_k\rangle\langle\varphi_k|\right) = \text{Tr}(\mathcal{O}\sigma), \quad (\text{A9})$$

which proves that Ω in Eq. (B3) is an unbiased estimator of \mathcal{O} . Note that Lemma 1 draws forth the relation

$$\bar{X}_\sigma = \sum_{k=1}^{d^2} c_k^\sigma \bar{X}_{|\varphi_k\rangle\langle\varphi_k|} \Leftrightarrow \sigma = \sum_{k=1}^{d^2} c_k^\sigma |\varphi_k\rangle\langle\varphi_k|, \quad (\text{A10})$$

then the last equality in Eq. (A9) follows. \square

The same results can be drawn with linear algebra. In the training phase, the k -th element of the target vector is

$$Y_k^{\text{tar}} = \langle\langle \mathcal{O} | \varrho_k \rangle\rangle, \quad (\text{A11})$$

where $\varrho_k = |\varphi_k\rangle\langle\varphi_k|$ is the density matrix of the k -th training state. Denote

$$\mathbf{M}_t = [|\varrho_1\rangle, |\varrho_2\rangle, \dots, |\varrho_{d^2}\rangle], \quad (\text{A12})$$

which is an invertible matrix, then

$$Y^{\text{tar}} = \langle\langle \mathcal{O} | \mathbf{M}_t \rangle\rangle. \quad (\text{A13})$$

Note that the matrix of training data satisfies

$$\mathbf{X}_t = [\bar{X}_{\varrho_1}, \bar{X}_{\varrho_2}, \dots, \bar{X}_{\varrho_{d^2}}] = \mathcal{T} \mathbf{M}_t. \quad (\text{A14})$$

Thus, the weight vector is

$$W = Y^{\text{tar}} \mathbf{X}_t^{-1} = \langle\langle \mathcal{O} | \mathcal{T}^{-1} \rangle\rangle, \quad (\text{A15})$$

where

$$\mathcal{T} = \mathbf{X}_t \mathbf{M}_t^{-1}. \quad (\text{A16})$$

Finally, we obtain

$$W \bar{X}_\sigma = \langle\langle \mathcal{O} | \sigma \rangle\rangle = \text{Tr}(\mathcal{O}\sigma). \quad (\text{A17})$$

In the training of pair-wise interacting reservoirs, we do not require the entire matrix \mathcal{T} , instead, we obtain the pair-wise matrix $\mathcal{T}_{\text{p.w.}}$, and decompose the n -qubit observable \mathcal{O} into a tensor product structure:

$$\mathcal{O} = \sum_i \bigotimes_{j=1}^n \mathcal{O}_{i,j}, \quad (\text{A18})$$

then the weight vector is

$$W = \langle\langle \mathcal{O} | \mathcal{T}^{-1} = \sum_i \bigotimes_j \mathcal{W}_{i,j}, \quad (\text{A19})$$

where $\mathcal{W}_{i,j} = \langle\langle \mathcal{O}_{i,j} | \mathcal{T}_{\text{p.w.}}^{-1}$. To reduce the complexity in classical post-processing, one only stores the set of two-node weights $\{\mathcal{W}_{i,j}\}$. Note that the single copy readout X shares the same tensor product structure, $X = \bigotimes_j \mathcal{X}_j$, where \mathcal{X}_j is a 4×1 dimensional vector. Denote

$$\hat{\Omega}_{i,j} = \mathcal{W}_{i,j} \cdot \mathcal{X}_j, \quad (\text{A20})$$

then the single-copy estimator is

$$\hat{\Omega} = \sum_i \prod_j \hat{\Omega}_{i,j}. \quad (\text{A21})$$

Thus, the classical storage consumption, i.e., $\{\mathcal{W}_{i,j}\}$ and $\{\mathcal{X}_j\}$, scales linearly with the number of qubits for observables that can be expressed as low-rank tensors.

Appendix B: Efficiency for estimating linear functions

Here we provide a method for analyzing the efficiency of QRPE in the worst-case scenario, which relies on the prior knowledge of the training data and the target parameters.

1. single-snapshot estimator

For a single input copy σ , the corresponding readouts can be combined into unbiased estimators of compatible parameters. The efficiency of the QRPE scheme is characterized by the variance of the estimators.

Lemma 2. *For a parameter \mathcal{O} , construct the single-snapshot estimator $\hat{\Omega}$ with the training data. Then in the worst-case scenario, we have*

$$\max_{\sigma} \text{Var}(\hat{\Omega}) \leq F_{\text{res}}(\mathcal{O}, \mathbf{X}_t), \quad (\text{B1})$$

where the function F_{res} depends on the training data:

$$F_{\text{res}}(\mathcal{O}, \mathbf{X}_t) = \max_{\substack{\sigma \succeq 0 \\ \text{Tr}(\sigma)=1}} W \odot W \bar{X}. \quad (\text{B2})$$

Proof. The single-snapshot estimator $\hat{\Omega}$ is a linear combination of the measurement results of mutually exclusive readout operators $\{\hat{o}_i\}$ with the corresponding weights $\{w_i\}$, i.e.,

$$\hat{\Omega} \equiv W \cdot \hat{X} = \sum_{i=1}^{N_{\text{read}}} w_i \hat{x}_i. \quad (\text{B3})$$

Thus, the expectation of $\hat{\Omega}$ is the inner product between W and \bar{X} . The variance of $\hat{\Omega}$ is

$$\begin{aligned} \text{Var}(\hat{\Omega}) &= \text{Var}\left(\sum_i w_i \hat{x}_i\right) \\ &= \sum_i w_i^2 \text{Var}(\hat{x}_i) + \sum_{i \neq j} w_i w_j \text{Cov}(\hat{x}_i, \hat{x}_j) \\ &= \sum_i w_i^2 \langle \hat{o}_i \rangle - \sum_{i,j} w_i w_j \langle \hat{o}_i \rangle \langle \hat{o}_j \rangle \\ &= W \odot W \bar{X} - (W \bar{X})^2, \end{aligned} \quad (\text{B4})$$

where \odot represents the Hadamard product. Thus,

$$\max_{\bar{X} \in \mathcal{C}} \text{Var}(\hat{\Omega}) \leq \max_{\substack{\sigma \succeq 0 \\ \text{Tr}(\sigma)=1}} W \odot W \bar{X}, \quad (\text{B5})$$

where we have neglected the term $-(W \bar{X})^2$. The inequality saturates when $\text{Tr}(\mathcal{O}\sigma) = 0$. \square

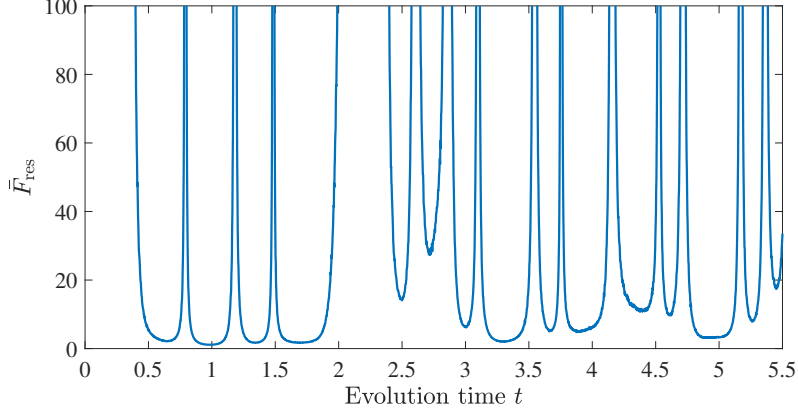


FIG. 8. Average variance upper bound of single-qubit state fidelity estimation that varies with evolution time from $t = 0$ to $t = 5.5$. The parameters J, P_i, E_i are the same with main text. At each evolution time, the variance upper bound for pure state fidelity estimation \bar{F}_{res} is averaged over 1000 random target states. While there are multiple local minimums with different slopes at neighboring points, the performance of reservoir parameters remains stable for a short time period at some local minimums.

Since we have $W = \langle\langle \mathcal{O} | \mathcal{T}^{-1}$ and $X = \mathcal{T} | \sigma \rangle\rangle$, we can directly compute the factor F_{res} . Define an operator \mathcal{B} such that

$$\langle\langle \mathcal{B} | \mathcal{T}^{-1} = \langle\langle \mathcal{O} | \mathcal{T}^{-1} \odot \langle\langle \mathcal{O} | \mathcal{T}^{-1}, \quad (\text{B6})$$

then

$$F_{\text{res}} = \max_{\substack{\sigma \succeq 0 \\ \text{Tr}(\sigma)=1}} \text{Tr}(\mathcal{B}\sigma) = \|\mathcal{B}\|_{\infty} \quad (\text{B7})$$

where $\|\cdot\|_{\infty}$ represents the spectral norm. Also, it is worth noting that estimating identity operator doesn't affect the variance. Define $\hat{\Omega}' = (W + cW_{\mathbb{1}})\hat{X}$, where $W_{\mathbb{1}} = [1, 1, \dots, 1]$ is the weight operator for the identity observable, and $c \in \mathbb{R}$. Since $c_1 W_{\mathcal{O}_1} + c_2 W_{\mathcal{O}_2} = W_{c_1 \mathcal{O}_1 + c_2 \mathcal{O}_2}$, $\hat{\Omega}'$ is the estimator for $\mathcal{O}' = \mathcal{O} + c\mathbb{1}$. Note that $\text{Var}(\hat{\Omega}) = \mathbb{E}[(\hat{\Omega} - \mathbb{E}(\hat{\Omega}))^2]$, and by construction $\sum_i \hat{x}_i = 1$, we have $\text{Var}(\hat{\Omega}') = \text{Var}(\hat{\Omega})$. We observe that $\hat{\Omega}_0$ results in a tighter worst-case variance upper bound on average in fidelity estimation of random pure target states. Also, for parameters that only differs by a product factor c ,

$$F_{\text{res}}(c\mathcal{O}, \mathbf{X}_t) = c^2 F_{\text{res}}(\mathcal{O}, \mathbf{X}_t). \quad (\text{B8})$$

With these properties, we note that if a reservoir setting works relatively better for overlap estimation of a target state σ , one could expect that it works better for estimating arbitrary linear parameters that can be decomposed as

$$\mathcal{O} = c_1 \sigma + c_2 \mathbb{1}, \quad c_{1,2} \in \mathbb{R}. \quad (\text{B9})$$

An arbitrary normal matrix is related to a density matrix by Eq. (B9). Thus, a well trained reservoir setting for overlap estimation of random target states is applicable to the future estimation of multiple unknown normal matrices. In order to analyze the search of good reservoir parameters, we fix the reservoir parameters $\{J, P_i, E_i\}$ and check the dependency of reservoir performance on evolution time. For the evolution time from $t = 0$ to $t = 5.5$, the variance upper bound of single-qubit state fidelity estimation averaged for 300 random target pure states varies, as shown in Fig. 8. It can be observed that the average variance upper bound is stable around some local minimums in a short time window.

Furthermore, we could analyze the efficiency scaling of estimating k -local observables with the help of pair-wise reservoir dynamics. Here we present the detailed proof for Theorem 2.

Lemma 3 (Theorem 2). *For a k -local parameter, e.g.*

$$\mathcal{O} = \bigotimes_{i=1}^k \mathcal{O}_i \bigotimes_{i=k+1}^n \mathbb{1}_i. \quad (\text{B10})$$

The worst-case variance upper bound is the product of that of each local parameters, i.e.,

$$\|\mathcal{B}\|_\infty = \prod_{i=1}^k \|\mathcal{B}_i\|_\infty. \quad (\text{B11})$$

Proof. Suppose the parameter \mathcal{O} is k -local, without loss of generality, we have

$$\mathcal{O} = \bigotimes_{i=1}^k \mathcal{O}_i \bigotimes_{i=k+1}^n \mathbb{1}_i. \quad (\text{B12})$$

Note that $W = \langle\langle \mathcal{O} | \mathcal{T}^{-1}, \bar{X} = \mathcal{T} | \sigma \rangle\rangle$ and $\mathcal{T} = \bigotimes_{i=1}^n \mathcal{T}_p$, there is

$$\max_{\substack{\sigma \succeq 0 \\ \text{Tr}(\sigma)=1}} W \odot W \bar{X} = \max_{\substack{\sigma \succeq 0 \\ \text{Tr}(\sigma)=1}} \bigotimes_{i=1}^k \langle\langle \mathcal{O}_i | \mathcal{T}_p^{-1} \odot \langle\langle \mathcal{O}_i | \mathcal{T}_p^{-1} \bigotimes_{i=k+1}^n W \mathbb{1}_i \mathcal{T} | \sigma \rangle\rangle. \quad (\text{B13})$$

Suppose the observable corresponding to the weight operator $\langle\langle \mathcal{O}_i | \mathcal{T}_p^{-1} \odot \langle\langle \mathcal{O}_i | \mathcal{T}_p^{-1}$ is \mathcal{B}_i , i.e.,

$$\langle\langle \mathcal{O}_i | \mathcal{T}_p^{-1} \odot \langle\langle \mathcal{O}_i | \mathcal{T}_p^{-1} = \langle\langle \mathcal{B}_i | \mathcal{T}_p^{-1}, \quad (\text{B14})$$

then

$$\max_{\substack{\sigma \succeq 0 \\ \text{Tr}(\sigma)=1}} W \odot W \bar{X} = \max_{\substack{\sigma \succeq 0 \\ \text{Tr}(\sigma)=1}} \text{Tr} \left(\bigotimes_{i=1}^k \mathcal{B}_i \bigotimes_{i=k+1}^n \mathbb{1}_i \sigma \right) = \left\| \bigotimes_{i=1}^k \mathcal{B}_i \bigotimes_{i=k+1}^n \mathbb{1}_i \right\|_\infty = \prod_{i=1}^k \|\mathcal{B}_i\|_\infty, \quad (\text{B15})$$

where $\max_{\substack{\sigma \succeq 0 \\ \text{Tr}(\sigma)=1}} W \odot W \bar{X} = \|\mathcal{B}\|_\infty$ is the worst-case variance upper bound for the single-snapshot estimator. \square

2. Multi-snapshot estimator

The variance can be further suppressed by combining single-snapshot estimators with statistical methods. The median of means method is expected to reduce the effect of outliers [4, 40], the efficiency of which is given by the following theorem.

Lemma 4. For target parameters $\{\mathcal{O}_i | i = 1, 2, \dots, M\}$ and training data \mathbf{X}_t , set

$$N_{\text{sample}} = 68/\epsilon^2 \ln(2M/\delta) \max_i F_{\text{res}}(\mathcal{O}_i, \mathbf{X}_t). \quad (\text{B16})$$

Then, consuming N_{sample} i.i.d. copies of input states suffice to construct median of means estimators $\{\hat{\Omega}_{\text{MoM},i}\}$, satisfying

$$|\hat{\Omega}_{\text{MoM},i} - \text{Tr}(\mathcal{O}_i \sigma)| \leq \epsilon \quad \text{for } i = 1, 2, \dots, M, \quad (\text{B17})$$

with probability no less than $1 - \delta$.

Proof. Divide the N_{sample} readouts into K batches, where

$$K = 2 \ln(2M/\delta). \quad (\text{B18})$$

Compute the sample mean estimator of each patch:

$$\hat{\Omega}_{\text{M},i}^{(k)} = \frac{K}{N_{\text{sample}}} \sum_{j=1}^N W_i X_j^{(k)}, \quad k = 1, 2, \dots, K, \quad (\text{B19})$$

then the median of means estimator is

$$\hat{\Omega}_{\text{MoM},i} = \text{Median}(\hat{\Omega}_{\text{M},i}^{(1)}, \hat{\Omega}_{\text{M},i}^{(2)}, \dots, \hat{\Omega}_{\text{M},i}^{(K)}). \quad (\text{B20})$$

Lemma. 2 and the median of means method [4] guarantees that

$$\Pr(|\hat{\Omega}_{\text{MoM},i} - \text{Tr}(\mathcal{O}_i \sigma)| > \epsilon) < \frac{\delta}{M}. \quad (\text{B21})$$

Finally, the union bound shows that the overall confidence level to estimate M parameters is no less than $1 - \delta$. \square

3. Variance reduction via probabilistic time multiplexing

The dynamic nature of quantum reservoirs is exploited with probabilistic time multiplexing. For each input copy of the unknown state, the evolution time of the reservoir is randomly chosen from the set $\{t_1, t_2, \dots, t_{N_{\text{time}}}\}$ with a probability distribution $\{p_1, p_2, \dots, p_{N_{\text{time}}}\}$. The probability vector of readout operators after probabilistic time multiplexing (PTM) is

$$\bar{X}^{\text{ptm}} = \sum_{i=1}^{N_{\text{time}}} p_i \bar{X}(t_i). \quad (\text{B22})$$

Solve the following optimization

$$F(\mathcal{O}, \mathbf{X}_t^{\text{opt}}) = \min_{\{p_i\}} F(\mathcal{O}, \mathbf{X}_t^{\text{ptm}}), \quad (\text{B23})$$

we are likely to reach a better variance upper bound. Note that PTM does not require changing either the initialization parameters of the reservoir or the measurement setting. Since the PTM is a one-time optimization, in this work we search the good probability distributions with brute force, which is achieved by the following algorithm.

Algorithm 1 PTM

```

Given parameters  $\{\mathcal{O}_i \mid 1, 2, \dots, M\}$ .
Load training data  $\{\mathbf{X}_t(t_i) \mid i = 1, 2, \dots, N_{\text{time}}\}$ .
Generate  $j_{\text{max}}$  random probability distributions  $\{P_j\}$ , where  $P_j = \{p_i^j \mid i = 1, 2, \dots, N_{\text{time}}\}$ .
Calculate  $F_{\text{res},0} = \max_i F_{\text{res}}(\mathcal{O}_i, \sum_k p_k^1 \mathbf{X}_t(t_k))$ .
Set  $P_{\text{PTM}} = P_1$ .
for  $j = 2, 3, \dots, j_{\text{max}}$  do
    Calculate  $F_{\text{res},1} = \max_i F_{\text{res}}(\mathcal{O}_i, \sum_k p_k^j \mathbf{X}_t(t_k))$ .
    if  $F_{\text{res},1} < F_{\text{res},0}$  then
        Update  $P_{\text{PTM}} = P_j$  and  $F_{\text{res},0} = F_{\text{res},1}$ .
    end if
end for

```

One may find better heuristic methods for this optimization.

The QRPE protocol with PTM is altered as:

1. Perform a one-time estimation of the training states of a two-node reservoir and load the training data $\{\mathbf{X}_p(t_k)\}$ to classical memory.
2. Given parameters $\{\mathcal{O}_i\}$, calculate weights $\{W_i\}$ with the training data. Run the PTM algorithm to obtain P_{PTM} and Var_0 . Calculate N_{sample} with the given confidence $1 - \delta$ and additive error ϵ .
3. Process N_{sample} i.i.d. copies of the unknown state σ with QRP. For each copy the reservoir evolution time is randomly chosen from $\{t_k\}$ with the probability distribution P_{PTM} . Load the readouts $\{X_i\}$ to classical memory.
4. Calculate the estimated values $\{\tilde{\mathcal{O}}_i\}$ with the weights and readouts.

Numerical result shows that for random reservoir dynamics, the variance could be suppressed by PTM. For each target state, we use the training data collected at 2 different time points with a random reservoir initialization, and optimize the variance upper bound with PTM. After that, we could achieve a more efficient estimation performance, as shown in Fig. 9.

Appendix C: Estimation of nonlinear functions

In this section we analyze the estimation of nonlinear functions with the QRPE scheme.

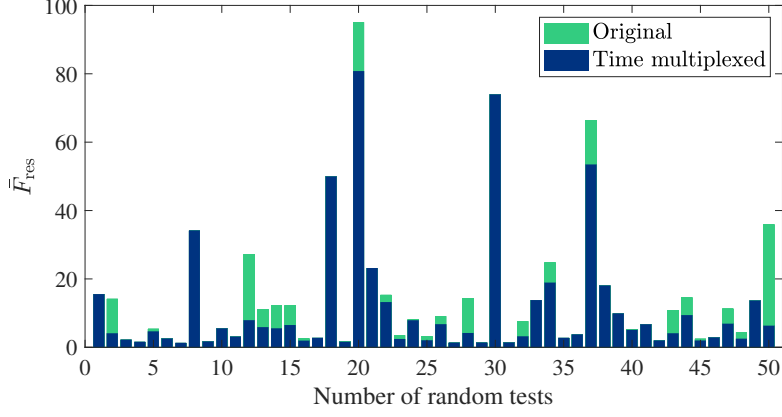


FIG. 9. Variance reduction via PTM. For each random test we use the training data collected at $t = 1$ and $t = 10$ of a two-node reservoir with parameters J, P_i, E_i uniformly generated at random from $[0, 5]$. The variance upper bound for overlap estimation \bar{F}_{res} is averaged over 300 random target states. The green bars uncovered by blue bars indicate the improvement in average variance upper bound achieved by PTM.

1. Unbiased estimator for nonlinear functions

The estimation of higher order moments, as stated in the main text, is reduced to estimating a linear function w.r.t. tensor product of the input state σ , i.e.,

$$\text{Tr}(\mathcal{O}\sigma^{\otimes m}) = \langle\langle \mathcal{O} | \sigma^{\otimes m} \rangle\rangle = \langle\langle \mathcal{O} | (|\sigma\rangle\rangle)^{\otimes m}, \quad (\text{C1})$$

where the second equality follows from the property of trace operation

$$\text{Tr}(A \otimes B) = \text{Tr}(A)\text{Tr}(B). \quad (\text{C2})$$

We estimate the expectation values of readout operators at an evolution time t ,

$$\mathbf{X} = [\bar{X}_{\varrho_1}, \bar{X}_{\varrho_2}, \dots, \bar{X}_{\varrho_{d^2}}] = \mathcal{T} \mathbf{M}_t. \quad (\text{C3})$$

The combined training data for estimating Eq. (C1) is

$$\mathbf{X}^{\otimes m} = \mathcal{T}^{\otimes m} \mathbf{M}_t^{\otimes m}, \quad (\text{C4})$$

and the target readout vector is

$$\mathbf{Y}^{\text{tar}} = \langle\langle \mathcal{O} | \mathbf{M}_t^{\otimes m}. \quad (\text{C5})$$

Thus, the weight vector is

$$\mathbf{W}^{(m)} = \mathbf{Y}^{\text{tar}} (\mathbf{X}^{\otimes m})^{-1} = \langle\langle \mathcal{O} | (\mathcal{T}^{\otimes m})^{-1}, \quad (\text{C6})$$

and the readout vector of an arbitrary input state σ satisfies

$$\bar{X}_{\sigma^{\otimes m}} = \mathcal{T}^{\otimes m} |\sigma\rangle\rangle^{\otimes m} = \bar{X}_{\sigma}^{\otimes m}. \quad (\text{C7})$$

In conclusion, we obtain

$$\mathbf{W}^{(m)} \bar{X}_{\sigma}^{\otimes m} = \langle\langle \mathcal{O} | \sigma \rangle\rangle^{\otimes m} = \text{Tr}(\mathcal{O}\sigma^{\otimes m}). \quad (\text{C8})$$

For simplicity, we will neglect the superscript of $\mathbf{W}^{(m)}$ when there is no ambiguity.

For pair-wise interaction, the classical resources consumed in the training phase is significantly reduced. Suppose the parameter is decomposed into

$$\mathcal{O} = \sum_i^n \bigotimes_{j=1}^m \bigotimes_{k=1}^m \mathcal{O}_{i,j,k}, \quad (\text{C9})$$

then the weight vector is

$$\mathbf{W} = \langle\langle \mathcal{O} | (\mathcal{T}^{\otimes m})^{-1} = \sum_i \bigotimes_j \mathbf{W}_{i,j}, \quad (\text{C10})$$

where $\mathbf{W}_{i,j} = \bigotimes_{k=1}^m \langle\langle \mathcal{O}_{i,j,k} | \mathcal{T}_s^{-1}$. Due to the tensor product structure of the single snapshot readout X , only $\mathbf{W}_{i,j,k}$ that correspond to nontrivial $\mathcal{O}_{i,j,k}$ are required in the classical post-processing.

2. Variance of U-statistics estimators

Suppose N copies of σ are injected to the reservoir and the corresponding readout vectors are $\{X_i | i = 1, 2, \dots, N\}$. The uniformly minimal-variance unbiased estimator (U-statistics estimator) for estimating $W\bar{X}_\sigma^{\otimes m}$ is

$$\hat{\Omega}^{(m)} = \frac{1}{P(N, m)} \sum_{i_1, i_2, \dots, i_m}^* W \bigotimes_{j=1}^m X_{i_j}, \quad (\text{C11})$$

where $P(N, m)$ is the m -permutations of N , \sum^* denotes the summation over all distinct subscripts, i.e., $\{i_1, i_2, \dots, i_m\}$ is an m -tuple of indices from the set $\{1, 2, \dots, N\}$ with distinct entries. The kernel of $\hat{\Omega}$ is a symmetric function

$$h(X_{i_1}, X_{i_2}, \dots, X_{i_m}) = \frac{1}{m!} \sum_{\{l_1, l_2, \dots, l_m\} \in \mathcal{P}(i_1, i_2, \dots, i_m)} W \bigotimes_{j=1}^m X_{l_j}, \quad (\text{C12})$$

where $\mathcal{P}(i_1, i_2, \dots, i_m)$ is the set that contains all permutations of i_1, i_2, \dots, i_m . Let

$$h_k(x_1, x_2, \dots, x_k) = \mathbb{E}[h(x_1, x_2, \dots, x_k, X_{k+1}, \dots, X_m)], \quad (\text{C13})$$

The variance for $\hat{\Omega}^{(m)}$ in Eq. (C11) is given by the Hoeffding's theorem [46]

$$\text{Var}(\hat{\Omega}^{(m)}) = \binom{N}{m}^{-1} \sum_{k=1}^m \binom{m}{k} \binom{N-m}{m-k} \text{Var}[h_k(X_1, X_2, \dots, X_k)]. \quad (\text{C14})$$

To estimate quadratic functions, the variance upper bound is given by Lemma S5 of Ref. [4]. Here we rephrase it as

Lemma 5. *The variance associated with $\hat{\Omega}^{(2)}$ satisfies*

$$\text{Var}(\hat{\Omega}^{(2)}) \leq \frac{8\mathcal{A}^{(2)}}{N}, \quad (\text{C15})$$

where

$$\mathcal{A}^{(2)} = \max \left(\text{Var}[W(X_1 \otimes \bar{X})], \text{Var}[W(\bar{X} \otimes X_2)], \sqrt{\text{Var}[W(X_1 \otimes X_2)]} \right). \quad (\text{C16})$$

Proof.

$$\begin{aligned} \text{Var}(\hat{\Omega}^{(2)}) &= \frac{2}{N(N-1)} \left[2(N-2)\text{Var}[h_1(X_1)] + \text{Var}[h_2(X_1, X_2)] \right] \\ &= \frac{1}{N(N-1)} \left[(N-2)\text{Var}[W(X_1 \otimes \bar{X} + \bar{X} \otimes X_2)] + \frac{1}{2}\text{Var}[W(X_1 \otimes X_2 + X_2 \otimes X_1)] \right] \end{aligned} \quad (\text{C17})$$

Note that $\text{Var}(A+B) \leq 2[\text{Var}(A) + \text{Var}(B)]$, we have

$$\begin{aligned} \text{Var}(\hat{\Omega}^{(2)}) &\leq \frac{2(N-2)}{N(N-1)} \left[\text{Var}[W(X_1 \otimes \bar{X})] + \text{Var}[W(\bar{X} \otimes X_2)] \right] \\ &\quad + \frac{2}{N(N-1)} \text{Var}[W(X_1 \otimes X_2)] \\ &\leq \frac{4}{N^2} \text{Var}[W(X_1 \otimes X_2)] + \frac{2}{N} \text{Var}[W(X_1 \otimes \bar{X})] + \frac{2}{N} \text{Var}[W(\bar{X} \otimes X_1)]. \end{aligned} \quad (\text{C18})$$

Then we have

$$\text{Var}(\hat{\Omega}^{(2)}) \leq \frac{4\mathcal{A}^{(2)}}{N} + \frac{4\mathcal{A}^{(2)^2}}{N^2}. \quad (\text{C19})$$

It is reasonable to assume $N > \mathcal{A}^{(2)}$, so we have $\text{Var}(\hat{\Omega}^{(2)}) \leq 8\mathcal{A}^{(2)}/N$. \square

Next, we could compute upper bounds for $\mathcal{A}^{(2)}$ with numerical methods. Define the matrix \mathbf{W}_{12} as

$$W \cdot (X_1 \otimes X_2) = X_1^T \mathbf{W}_{12} X_2 = \sum_{i=1}^{N_{\text{read}}} \sum_{j=1}^{N_{\text{read}}} w_{ij} X_1(i) X_2(j), \quad (\text{C20})$$

we have

$$\begin{aligned} \text{Var}[W(X_1 \otimes X_2)] &= \text{Var} \sum_{i=1}^{N_{\text{read}}} \sum_{j=1}^{N_{\text{read}}} w_{ij} \hat{x}_i \hat{x}_j \\ &= \sum_i \sum_j w_{ij}^2 \text{Var}(\hat{x}_i \hat{x}_j) + \sum_{(i,j) \neq (k,h)} w_{ij} w_{kh} \text{Cov}(\hat{x}_i \hat{x}_j, \hat{x}_k \hat{x}_h) \\ &\leq \sum_i \sum_j w_{ij}^2 \langle \hat{o}_i \rangle \langle \hat{o}_j \rangle = W \odot W \cdot \bar{X} \otimes \bar{X}. \end{aligned} \quad (\text{C21})$$

Also, there are

$$\begin{aligned} \text{Var}[W(X_1 \otimes \bar{X})] &= \text{Var} \sum_{i=1}^{N_{\text{read}}} \sum_{j=1}^{N_{\text{read}}} w_{ij} \langle \hat{o}_j \rangle \hat{x}_i \\ &= \sum_i \sum_k w_{ik} \langle \hat{o}_k \rangle \sum_h w_{ih} \langle \hat{o}_h \rangle \text{Var}(\hat{x}_i) + \sum_{i \neq j} \sum_k w_{ik} \langle \hat{o}_k \rangle \sum_h w_{jh} \langle \hat{o}_h \rangle \text{Cov}(\hat{x}_i, \hat{x}_j) \\ &\leq \sum_i \sum_k \sum_h w_{ik} w_{ih} \langle \hat{o}_k \rangle \langle \hat{o}_h \rangle \langle \hat{o}_i \rangle = \bar{X}^T (\mathbf{W}_{12} \bar{X}) \odot (\mathbf{W}_{12} \bar{X}), \end{aligned} \quad (\text{C22})$$

and similarly

$$\text{Var}[W(\bar{X} \otimes X_2)] \leq \sum_i \sum_k \sum_h w_{ki} w_{hi} \langle \hat{o}_k \rangle \langle \hat{o}_h \rangle \langle \hat{o}_i \rangle = (\bar{X}^T \mathbf{W}_{12}) \odot (\bar{X}^T \mathbf{W}_{12}) \bar{X}. \quad (\text{C23})$$

To conclude this section, we illustrate the median of U-statistics estimators [4] by the following lemma:

Lemma 6. For target parameters $\{\mathcal{O}_i | i = 1, 2, \dots, M\}$ and training data \mathbf{X}_t , set

$$N_{\text{sample}} = \frac{544}{\epsilon^2} \ln\left(\frac{2M}{\delta}\right) \max_i \mathcal{A}^{(2)}(\mathcal{O}_i, \mathbf{X}_t). \quad (\text{C24})$$

Then, consuming N_{sample} i.i.d. copies of input states suffice to construct median of U-statistics estimators $\{\hat{\Omega}_i^{(2)}\}$, satisfying

$$|\hat{\Omega}_i^{(2)} - \text{Tr}(\mathcal{O}_i \sigma^{\otimes 2})| \leq \epsilon \quad \text{for } i = 1, 2, \dots, M, \quad (\text{C25})$$

with probability no less than $1 - \delta$.

Proof. We divide the copies into $K = 2 \ln(2M/\delta)$ equal-sized sets, and compute the U-statistics estimators for each set. Then, the medians of U-statistics estimators are the final estimation results for the parameters. The property of median estimator ensures that if each U-statistic estimator has a variance no larger than $\epsilon^2/34$, then

$$\Pr\left[|\hat{\Omega}_i^{(2)} - \text{Tr}(\mathcal{O}_i \sigma^{\otimes 2})| \leq \epsilon\right] \geq 1 - 2e^{-K/2}. \quad (\text{C26})$$

Thus, for each $\hat{\Omega}_i^{(2)}$ the confidence level is no less than $1 - \delta/M$. The union bound ensures that the over all confidence level for estimating M parameters is no less than $1 - \delta$. From Lemma. 5, we choose the size for each set as $272/\epsilon^2 \max_i \mathcal{A}^{(2)}(\mathcal{O}_i, \mathbf{X}_t)$. Consequently, the total number of copies consumed is $N_{\text{sample}} = 544/\epsilon^2 \ln(2M/\delta) \max_i \mathcal{A}^{(2)}(\mathcal{O}_i, \mathbf{X}_t)$. \square